A Novel Inorganic Hollow Fiber Membrane Reactor for Catalytic Dehydrogenation of Propane

Zhentao Wu, Irfan M. D. Hatim, Benjamin F. K. Kingsbury, Ejiro Gbenedio, and K. Li
Dept. of Chemical Engineering, Imperial College London, London, SW7 2AZ, U.K

DOI 10.1002/aic.11864
Published online July 13, 2009 in Wiley InterScience (www.interscience.wiley.com).

A novel inorganic hollow fiber membrane reactor (iHFMR) has been developed and applied to the catalytic dehydrogenation of propane to propene. Alumina hollow fiber substrates, prepared by a phase inversion/sintering method, possess a unique asymmetric structure that can be characterized by a very porous inner surface from which finger-like voids extend across ~80% of the fiber cross-section with the remaining 20% consisting of a denser sponge-like outer layer. In contrast to other existing Pd/Ag composite membranes, where an intermediate γ-Al_2O_3 layer is often used to bridge the Pd/Ag layer and the substrate, the Pd/Ag composite membrane prepared in this study was achieved by coating the Pd/Ag layer directly onto the outer surface of the asymmetric substrate. After depositing submicron-sized Pt (0.5 wt %)/γ-alumina catalysts in the finger-like voids of the substrates, a highly compact multifunctional iHFMR was developed. Propane conversion as high as 42% was achieved at the initial stage of the reaction at 723 K. In addition, the space-time yields of the iHFMR were ~60 times higher than that of a fixed bed reactor, demonstrating advantages of using iHFMR for dehydrogenation reactions. *AIChE J,* 55: 2389–2398, 2009
Keywords: alumina hollow fiber, asymmetric structure, Pd/Ag membrane, membrane reactor, dehydrogenation of propane

Introduction

Because of the production of polypropylene from propene, the direct dehydrogenation of propane ($C_3H_8 \leftrightarrow C_3H_6 + H_2$, $\Delta H^\circ = 124$ kJ/mol) to propene has been extensively studied both theoretically and experimentally in the past several decades.[1,2] High temperatures (773–873 K) and low pressures (0.3–1 atm) are industrially used to obtain commercially acceptable conversions due to the endothermic nature of the reaction.[1] For instance, the conversion of propane in the Catofin™ process is between 48 and 65% per pass at 823 K when the operating pressures are at 0.3–0.5 bar.[1] Besides the considerable amount of extra energy needed, high operating temperatures promote undesirable side-reactions that quickly deactivate the catalysts. Severe coking is often observed and frequent catalyst regeneration after short time intervals of only 15–30 min is necessary.[1] In the case of the UOP Oleflex™ process, a longer cycle duration of about 7 h can be achieved at 823 K by adding hydrogen to the feed to reduce the coke formation, although propane conversion is limited to around 40% for thermodynamic reasons.[2]

The use of membrane reactors allows the continuous removal of hydrogen from the reaction zone during the dehydrogenation of propane to propene, thus offering the possibility of substantially increasing the conversion and/or lowering the reaction temperature in endothermic, equilibrium-limited reactions of this type.[3–5] Compared to porous membrane reactors, dense membrane reactors, such as Pd-

Correspondence concerning this article should be addressed to K. Li at kang.li@imperial.ac.uk

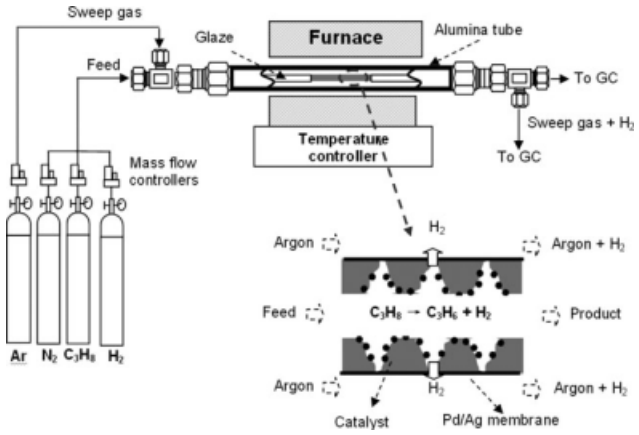

Figure 1. Schematic diagram of the apparatus for the dehydrogenation of propane to propene.

based membranes, possess much better performance because of its extremely high hydrogen selectivity.[5–7] Thin and defect-free Pd-based membranes are usually deposited onto porous ceramic or metal substrates to achieve high permeation flux, reduced membrane cost, sufficient mechanical strength, etc. without compromising the hydrogen permselectivity.[3,8] In most cases, Pd-based membranes cannot be directly deposited onto the porous substrates with symmetric structures because of their large surface pore size. As a result, a γ-Al_2O_3 intermediate layer, which is usually prepared by a sol–gel based technique, is widely used before the subsequent membrane deposition.[3,8]

After the report of the successful preparation of porous alumina hollow fibers with supremely high surface area/volume ratio,[9] various studies have been carried out to deposit Pd-based membranes onto the substrates of this type for hydrogen separation,[10–14] in which a γ-Al_2O_3 intermediate layer was often used as discussed previously. Although Tong et al.[15,16] developed a novel combined organic and inorganic process to avoid the need for the mechanically weak, intermediate γ-Al_2O_3 layer, a multistep post-treatment was still necessary. Alumina hollow fiber substrates with symmetric structures featured in a study of Sun et al.,[17] involving in elimination of finger-like voids of fibers for greater mechanical strength. No intermediate layer was required when a Pd membrane as thin as around 1.5 μm was deposited onto hollow fiber substrates consisting entirely of a sponge-like structure.

In contrast to the substrates used earlier, the alumina hollow fiber substrate prepared in this study possesses a unique asymmetric pore structure that is characterized by a very porous inner surface from which finger-like voids extend across $\sim$80% of the fiber cross-section with the remaining 20% consisting of a denser sponge-like outer layer. This unique structure confers several advantages, as the sponge-like outer layer with its narrow pore size distribution provides a sufficiently smooth surface for the direct deposition of a thin and defect-free hydrogen separation layer without any pre or post-treatment, while long finger-like voids in the substrate wall provide an extensive surface for the deposition of catalysts as shown in the insert of Figure 1.

In this study, Pd/Ag alloy membranes with the composition close to 77 wt % Pd and 23wt % Ag, which have been widely studied because of their great H_2 permeation flux and stability, have been selected as the H_2 separation layer and have been coated onto the denser sponge-like outer layer of the substrate, while submicron-sized Pt (0.5 wt %) γ-alumina catalyst particles have been deposited into the finger-like voids through the very porous inner surface, forming a highly compact multifunctional membrane reactor for simultaneous dehydrogenation of propane to propene and hydrogen separation. Because of the limitation on the stability of the catalyst, the operating temperature was inevitably fixed at 723 K at which the equilibrium conversion of propane is low. However, in comparison with the traditional fixed bed reactor (FBR), the highly compact multifunctional inorganic hollow fiber membrane reactor (iHFMR) proposed in this study clearly demonstrates its advantages.

Experimental

Materials

Aluminum oxide powders of 1 μm (alpha, 99.9% metals basis, S.A. 6–8 m^2/g), 0.05 μm (gamma-alpha, 99.5% metals basis, S.A. 32–40 m^2/g), and 0.01 μm (gamma-alpha, 99.98% metals basis, S.A. 100 m^2/g) particle sizes were purchased from Alfa Aesar and were used as supplied. Polyethersulfone (PESf, Radel A-300, Ameco Performance, USA), *N*-methyl-2-pyrrolidone (NMP, HPLC grade, Rathbone), and Arlacel P135 (Uniqema, UK) were used as binder, solvent, and additive, respectively. DI water and tap water were used as the internal and external coagulants, respectively, when fabricating Al_2O_3 hollow fiber precursors. $Pd(NH_4)_2Cl_4$ (Ammonium tetrachloropalladate, 99.99%, Aldrich), $SnCl_2{\cdot}2H_2O$, $Na_2EDTA{\cdot}2H_2O$, HCl (37%), N_2H_4, $AgNO_3$, and $NH_3{\cdot}H_2O$ (28%) (Fisher Sci. Ltd) were used for preparing the Pd/Ag hydrogen separation layer using an electroless plating (ELP) method. H_2PtCl_6 (99.995%, Aldrich) and gamma-aluminum oxide powders of 60 nm (99% metal basis, S.A. 180 m^2/g, Alfa Aesar) were used for preparing the Pt (0.5 wt %)/γ-Al_2O_3 catalyst using a traditional impregnation method.

Preparation of multifunctional membranes

Asymmetric Al_2O_3 Hollow Fiber Substrates. Asymmetric Al_2O_3 hollow fiber substrates were fabricated via a phase inversion/sintering technique.[9] Arlacel P135 (0.1 wt %/alumina surface area) was dissolved in NMP before the addition of aluminum oxide powders (1 μm: 0.05 μm: 0.01 μm = 7:2:1). The dispersion was rolled with 20-mm agate milling balls with an Al_2O_3/agate weight ratio of 1.9 for 48 h and milling was continued for a further 48 h after the addition of PESf. The spinning suspension was then transferred to a gas-tight reservoir and degassed under vacuum for 2 h. After degassing, the suspension was pressurized at 7–20 psig using nitrogen gas and was extruded through a tube-in-orifice spinneret (ID 1.2 mm, OD 3.0 mm) into a coagulation bath containing 120 l of water with an air-gap of 15 cm. DI water was used as the internal coagulant and the flow rate ranged from 10 to 30 ml/min. The formed precursor fibers were first heated in a CARBOLITE tube furnace at about 873 K for 2 h to remove the organic polymer binder and were then

Table 1. Coating Bath Compositions of Pd/Ag Electroless Plating

Compounds	Pd Bath	Ag Bath
$Pd(NH_3)_4Cl_2 \cdot H_2O$ (g/l)	4	–
$AgNO_3$ (g/l)	–	0.519
$Na_2EDTA\ 2H_2O$ (g/l)	40.1	40.1
NH_4OH (28%) (ml/l)	198	198
N_2H_4(1 M) (ml/l)	5.6	5.6
pH	10–11	10–11
Temperature (K)	333	333

sintered at 1723 K for 4 h with heating and cooling rates of 5 K/min. The outer surface of the prepared substrates (about 30 cm in length after sintering) was coated with a thin and gas-tight layer of glaze with the exception of the central part of the fiber (of around 5 cm in length) being left for ELP of Pd/Ag membrane.

Catalyst Preparation and Deposition. Submicron-sized Pt (0.5 wt %)/γ-Al_2O_3 catalyst was prepared by impregnation of γ-Al_2O_3 powders of 60 nm with the aqueous solution of H_2PtCl_6 at room temperature. After impregnation, the catalyst was dried at 383 K overnight and calcined at 773 K for 4 h with heating and cooling rates of 2 K/min. Before catalyst deposition, the catalyst was reduced under flowing H_2 at 773 K for 2 h. The deposition of the catalyst particles into the finger-like voids of the substrates was performed by uniformly dispersing the prepared catalyst in an aqueous medium using Arlacel P135 as a dispersant first. The hollow fiber substrates were vacuumed for 1 h to remove the air trapped inside. A volume of the suspension containing catalyst particles was then sucked into a closed vessel containing the substrates. After 1 h, the vessel was opened to the atmosphere which applied an additional driving force for the suspension to penetrate into the finger-like voids within the substrates. Before drying the substrates in an oven overnight at 383 K, the remaining suspension in the substrate lumen was expelled using compressed air. This catalyst deposition process was repeated three times for sufficient loading of catalyst in the finger-like voids before the dehydrogenation reaction.

Pd/Ag Coating. The Pd/Ag membranes were coated onto the outer surface of asymmetric alumina hollow fiber substrates by an ELP technique.[3] Before the coating, the substrates were cleaned and activated by the conventional Pd-Sn activation procedure. The activation process consisted of successive immersion of the substrates in the tin (II) chloride ($SnCl_2$) solution and the palladium chloride ($PdCl_2$) solution at room temperature. Deionized water and 0.1 M HCl were used to rinse the samples between the immersions. The activation process was repeated six times, after which the substrate surface turned brown. The Pd/Ag membrane was then coated by a "coating-diffusion" process[3] using the plating baths having the compositions shown in Table 1. Before the Ag coating, a Pd layer was coated onto the activated substrate surface. The thicknesses of the Pd and the Ag layer were determined by controlling the plating process, in which the plating solution was refreshed every hour. The homogeneous Pd/Ag alloy membrane was obtained by heat treatment of the samples at 923 K for 12 h.

Characterization of multifunctional hollow fiber membranes

The morphology of the alumina hollow fiber substrates, the Pd/Ag composite membranes, and the catalyst deposited in the finger-like voids were visually observed using a scanning electron microscope (JEOL JSM-5610LV, Tokyo, Japan). A clear cross-sectional fracture of hollow fiber substrates was obtained by directly snapping the samples. All the samples were positioned on a metal holder and gold coated using sputter-coating operated under vacuum. The SEM micrographs of both the sample surface and the cross-section were taken at various magnifications. EDS analysis (INCA Energy by Oxford Instruments) was used to investigate the elemental distribution across the Pd/Ag membranes.

Single gas (H_2 or N_2) permeation measurements of both the asymmetric Al_2O_3 hollow fiber substrates with and without catalyst loading and the Pd/Ag composite membranes were carried out. The gas permeation module was placed into a CARBOLITE tube furnace equipped with a microprocessor temperature controller. The effective heating zone of constant temperature was ~5 cm of length. Pressurized hydrogen or nitrogen (99.99%) was introduced into the shell of the module. The operating pressures were adjusted by a pressure regulator (PRG-101-60, Omega) and monitored using a KN2200 electronic pressure gauge. The pressure in the lumen was kept at atmospheric pressure. The flow rates of gas permeating through the substrates or the Pd/Ag composite membranes were measured using bubble flow meters.

Dehydrogenation of propane to propene

The apparatus for the dehydrogenation of propane to propene is schematically shown in Figure 1. A gaseous stream containing propane (5%) and hydrogen (4.5%) with balanced nitrogen was introduced at 30 ml/min into the lumen of the reactor. Argon with a flow rate of 50 ml/min was used as a sweep gas to carry the permeated hydrogen to a TCD gas chromatograph (Varian-3900) for analysis. The membrane reactor was operated at atmospheric pressure and the effluent gases from the reactor were analyzed online using a FID gas chromatograph (Varian-3900). It should be noted that the above operation is only used for lab-scaled apparatus. For a commercial unit, it would be logical to use vacuum instead of using Ar as a sweep gas. Also, the iHFMRs would be constructed with a bundle of the fibers instead of a single fiber to obtain a surface area/volume ratio for commercial applications.

Results and Discussion

Microstructure of asymmetric Al_2O_3 hollow fiber substrates

Figure 2 shows morphologies of the asymmetric Al_2O_3 hollow fiber substrates sintered at 1723 K for 4 h. The OD and ID of the fibers with uniform wall thickness were measured at ~1893 μm and 964 μm, respectively. As can been seen, the hollow fiber substrates prepared possess a unique asymmetric structure composed of long finger-like voids and a thin and uniform sponge-like layer (Figures 2a, b) with a very porous inner surface (Figure 2c) and a relatively denser

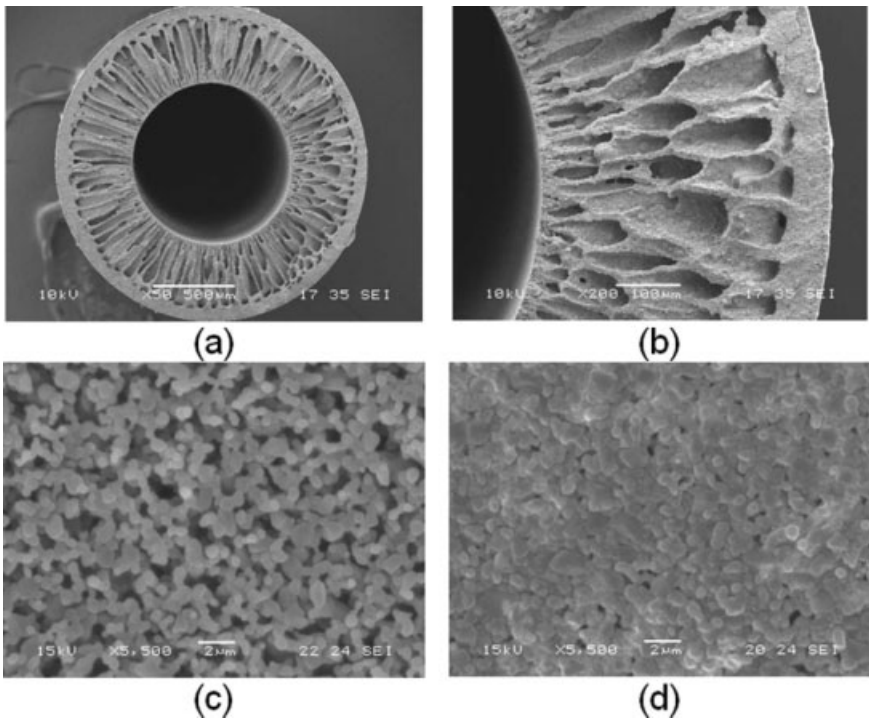

Figure 2. SEM images of the asymmetric alumina hollow fiber substrate sintered at 1723 K for 4 h: (a) whole view, (b) cross section, (c) inner surface, and (d) outer surface.

outer surface (Figure 2d). The formation of finger-like voids at the inner fiber surface is believed to be initiated by instabilities at the interface between the nonsolvent and the suspension. Finger-like void growth then proceeds as a result of nonsolvent influx into the suspension as a result of the viscous fingering phenomenon. Because of the high concentration of nonsolvent at the interface, polymer precipitation is instantaneous resulting in a rapid, large increase in the viscosity of the suspension in this region. Consequently, the suspension viscosity exceeds the critical value at which further morphological change may take place and the size of the entrances to the finger-like voids is determined at this point. Nonsolvent influx through these entrances into the suspension results in finger-like void growth. However, the polymer precipitation rate within the suspension is lower than that at the interface with nonsolvent due to the lesser availability of nonsolvent in this region. As a result, the suspension viscosity remains below the critical value for longer and finger-like void growth may proceed, giving rise to the characteristic finger-like shape. Finger-like void growth cannot proceed above a critical suspension viscosity and consequently growth is halted when this value is exceeded. Exposure of the outer fiber surface to the atmosphere causes an increase in viscosity in this region due to simultaneous solvent evaporation and nonsolvent condensation from the surrounding atmosphere. For fibers prepared as substrates in this work, the critical suspension viscosity is exceeded in the outer region of the fiber before immersion in nonsolvent takes place. Consequently, finger-like void growth is not observed at the outer fiber surface and a sponge-like structure results.

Accompanied by the growth of the finger-like voids, a highly porous inner surface and a relatively denser outer surface are formed as shown in Figures 2c, d. In contrast to other existing alumina substrates with symmetric structures, the sponge-like layer near the outer wall prepared in this study is much thinner. In addition, the usage of fine particles contributes to both the narrow pore size distribution and the sufficiently smooth outer surface for the direct deposition of Pd/Ag membranes. Moreover, catalyst could be deposited into the finger-like voids of the substrates. Thus, highly compact multifunctional membranes can be further fabricated.

Catalyst preparation and deposition

Submicron-sized Pt (0.5 wt %)/γ-alumina catalyst was prepared using a traditional impregnation method and deposited into the substrate of hollow fiber membrane reactor (iHFMR). Before catalyst deposition, the catalyst particles were dispersed in an aqueous medium using Arlacel P135 as a dispersant. Only the catalyst particles suspended evenly in the aqueous medium were used for subsequent catalyst deposition. As a result, a very small amount of the catalyst was deposited uniformly in the finger-like voids of the asymmetric alumina substrates. As can be seen from Figure 3a, the surfaces of the finger-like voids were covered by a thin layer of submicron-sized catalyst particles, while the sponge-like regions of the substrate remained unaffected. Figure 3b shows the finger-like void surface at high magnification and indicates that the catalysts are sparsely deposited on the surface of the finger-like voids. This agrees with the result that, after the catalyst deposition, the average weight gain of the

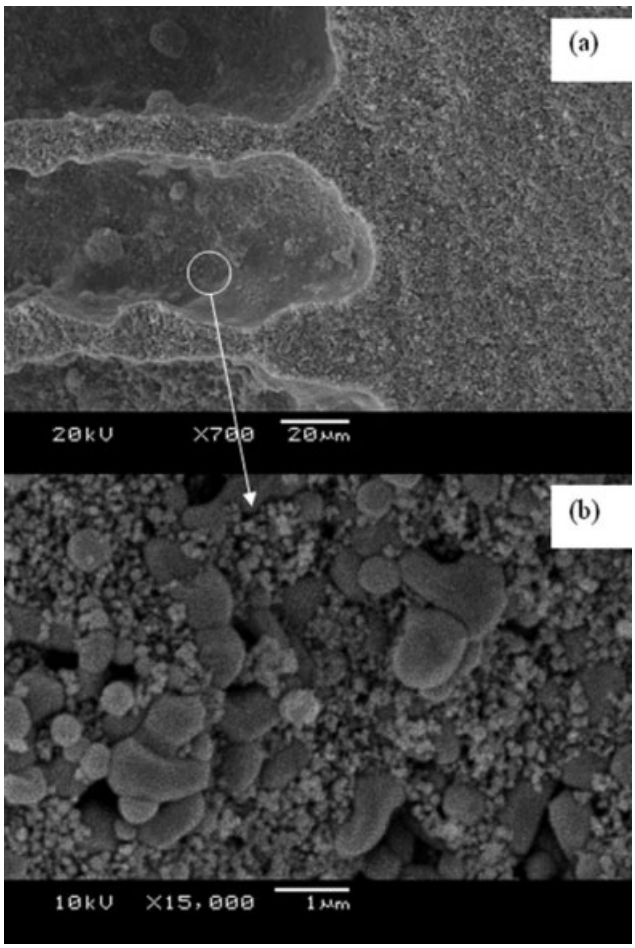

Figure 3. SEM images of catalyst deposition in the hollow fiber substrate: (a) catalyst particles deposited into the finger-like voids and (b) finger-like voids with high magnification.

asymmetric alumina hollow fiber substrates (30 cm in length) is only ~0.74%, as listed in Table 2.

Gas permeation of Al_2O_3 hollow fiber substrates

The permeation characteristics of Al_2O_3 hollow fiber substrates were investigated using H_2 and N_2 gas permeation measurements. The permeation results are shown in Figure 4. As can be seen, the permeances of H_2 and N_2 slightly increase as the mean pressure across the substrates is increased, indicating that the total flow through the alumina hollow fiber substrates (sintered at 1723 K for 4 h) is described by the combined contribution of Knudsen diffusion

Table 2. The Weight Gain of the Asymmetric Alumina Hollow Fiber Substrates After Catalyst Deposition

Catalyst Deposition	Whole Weight of Samples (mg)	Weight Gain (%)
Before deposition	935.6	–
After 1st 1 h deposition	936.5	0.10
After 2nd 1 h deposition	940.4	0.51
After 3rd 1 h deposition	942.5	0.74

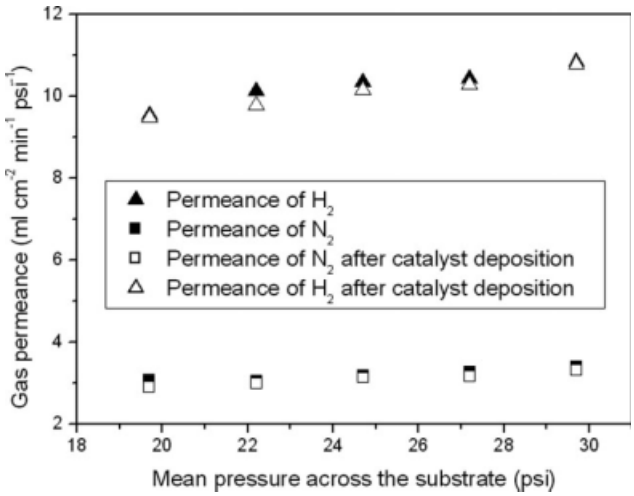

Figure 4. Gas permeation of hydrogen and nitrogen through the hollow fiber substrates at room temperature.

and Poiseuille flow.[17,18] The separation factor (α) of H_2/N_2 was measured to be 3.2, which is slightly lower than those of 3.3–3.5 achieved by modifying the substrates with a γ-Al_2O_3 intermediate layer.[3,17] Figure 4 further illustrates that the H_2 and N_2 permeation fluxes of the substrates with and without the catalyst are very close, indicating that the mass transfer resistance created due to the catalyst deposition is negligible.

Sequential electroless plating of Pd/Ag membranes

The Pd/Ag composite membranes were coated onto the outer surface of the substrates prepared above by a ''coating-diffusion'' ELP method[3] where the plating bath was refreshed every 1 h. Before the deposition of Ag, the surface of the Pd membrane was reactivated so as to produce uniform Ag plating. The composition of the Pd/Ag membranes was controlled by the plating rates of Pd and Ag as shown in Figure 5. The weight gain of Pd and Ag increases linearly

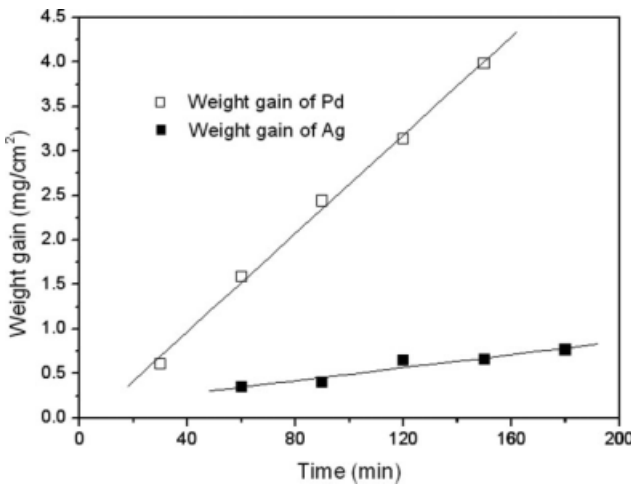

Figure 5. Weight gain of Pd and Ag during the electroless plating.

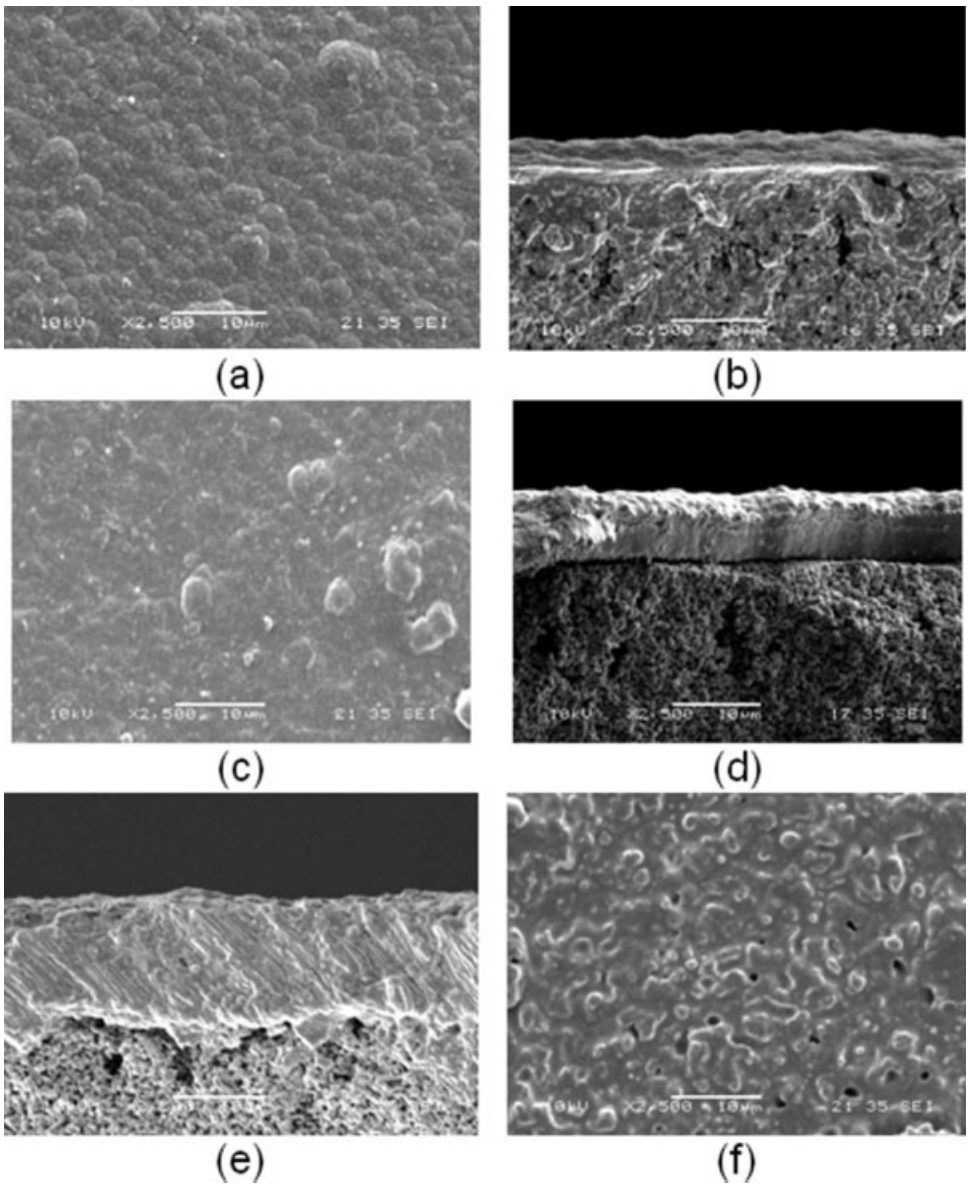

Figure 6. SEM images of Pd/Ag composite membranes during "coating and diffusion" electroless plating: (a) surface of Pd layer, (b) cross-section of Pd layer, (c) surface of Ag layer, (d) cross-section of Pd and Ag layers before heat treatment, (e) cross-section of Pd/Ag alloy after heat treatment, and (f) surface of Pd/Ag alloy after heat treatment.

with time during the ELP. The mechanism of the ELP technique is based on the controlled autocatalytic reduction of the metastable metallic salt complexes on the target surfaces.[19] Nonlinear behavior can be observed when the ELP is carried out continuously without changing the ELP solution, in which the number of the Pd nucleation sites and the concentration of the metallic salt complexes change with time. In contrast, the ELP solution in this study was refreshed every hour, as a result of which the Pd and Ag plating behaviors were linear with respect to time. The plating rate of Pd is ~6.5 times higher than that of Ag. This plating profile was further confirmed by preparing Pd/Ag membranes with different thicknesses, which were calculated based on the theoretical densities of Pd and Ag. The calculated membrane thicknesses agree well with that of the SEM characterizations.

Figure 6 shows the morphology of a Pd/Ag membrane with the thickness around 8 μm. The reason for choosing a relatively thick membrane for SEM as well as the subsequent EDS analysis is to highlight the microstructural change of the membranes during the ELP process. As can be seen from Figures 6a, b, a uniform Pd layer was first deposited on the activated substrate with the Pd grains tightly bound on the surface without observable defects. A less defined grain boundary on the surface of the Ag layer is shown in Figure 6c. A clear double-layer structure was obtained after the deposition of Ag as shown in Figure 6d. Figure 6e illustrates that the boundary between the Pd and the Ag layers

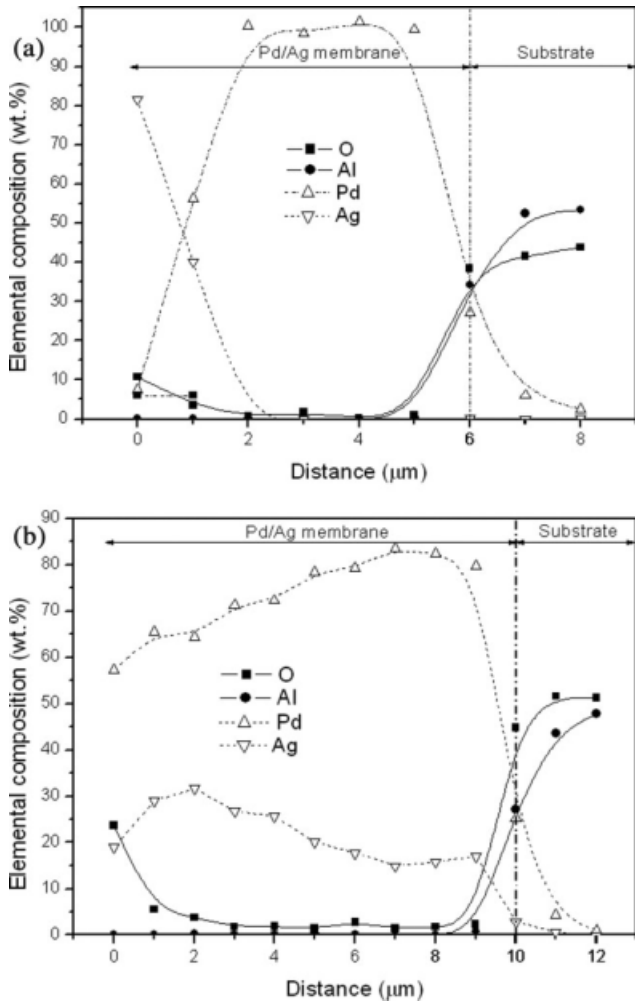

Figure 7. EDS analysis of Pd/Ag membranes: (a) before heat treatment and (b) after heat treatment.

disappeared after heat treatment at 923 K for 12 h in Ar due to intermetallic diffusion between the layers. Although some small pores were found on the surface of the composite membrane after the heat treatment (Figure 6f), these pores are dead volumes, as the membrane as a whole is gas-tight with excellent H_2/N_2 selectivity.

EDS analysis was also carried out to investigate the elemental distribution across the Pd/Ag membrane cross-section before and after heat treatment. As shown in Figure 7a, a small amount of Pd was observed at $\sim$2 μm beneath the substrate surface before heat treatment, which indicated that the Pd plating solution penetrated slightly into the substrate during the ELP process. In contrast to Figure 7a, significant change in the elemental distribution across the membrane occurred after heat treatment as shown in Figure 7b. The Tamman temperature (TM) is defined as the temperature at which considerable thermal vibration occurs in a lattice and is estimated at half the melting point (K) of a material.[20] As the TM of Ag, which is about 617 K, is much lower than that of Pd (914 K), it is reasonable to assume that silver atoms migrate significantly into the palladium layer during heat treatment. As can be seen in Figure 7b, the concentration of Ag decreased slightly toward the substrate, while the concentration of Pd was increased. This indicates that a higher temperature and/or longer time would be required for a more uniform elemental distribution in such a thick membrane. Although a number of researches on metallic interdiffusions have been carried out to determine the diffusion coefficient of Ag in Pd, it is still difficult to accurately predict the alloying process. For example, the diffusion coefficients from several groups are quite different from each other.[20] One of the possible reasons is that, apart from the material nature of Pd and Ag, the alloying process can be determined by the membrane microstructure, which is closely related to the preparation processes and the surface property of the substrates. Hou and Hughes[21] obtained homogeneous Pd/Ag membranes by annealing the membrane at 873 K for 10 h, which is quite similar to our work. While Uemiya et al.[22] concluded that high temperatures of above 1073 K were necessary to obtain a homogeneous Pd/Ag alloy membrane. However, area scans performed randomly on the cross section of other thinner samples revealed an average Pd/Ag ratio of 78:22, which was considered to be an indication that the Pd/Ag membranes used in subsequent experiments have a homogeneous distribution of Pd and Ag.

Gas permeation of Pd/Ag-Al_2O_3 composite hollow fiber membranes

Figure 8 shows the effect of the pressure difference on hydrogen permeation through a 5 μm Pd/Ag composite membrane between 723 and 873 K. Before the introduction of hydrogen, the sealing of the module and the gas-tightness of the composite membrane were tested using nitrogen with the transmembrane pressure up to 3 bar. A 1 ml bubble flow meter with a minimum detectable scale of 0.01 ml was used to measure the flow rate of nitrogen. No soap bubble movement was observed at every operating temperature and pressure, indicating that the hydrogen/nitrogen selectivity in this research is close to infinity. In addition, a technique for

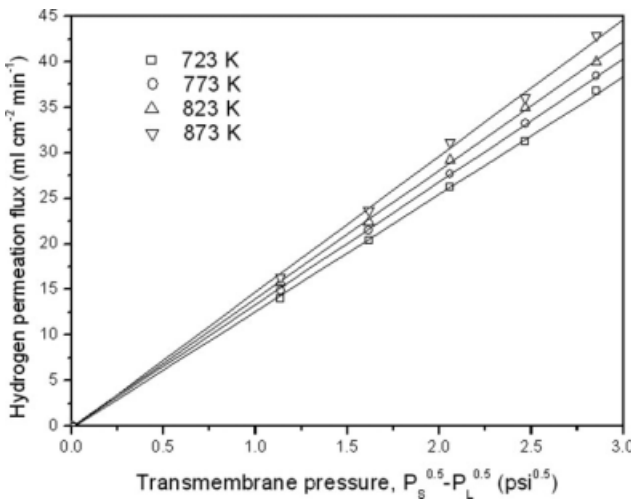

Figure 8. Relationship between square root of pressure difference and hydrogen permeation flux through Pd/Ag composite membrane at different temperatures.

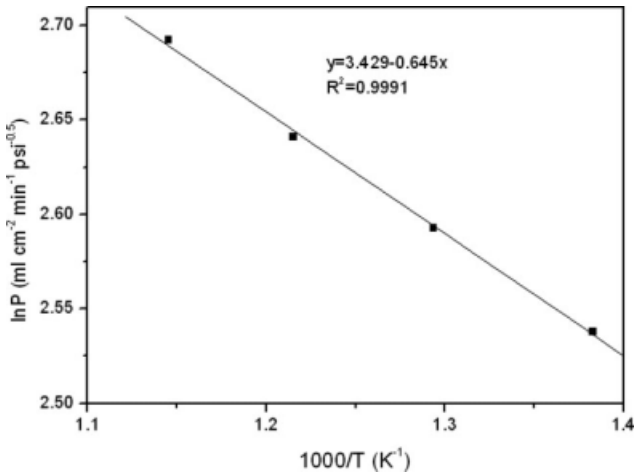

Figure 9. Arrhenius plot of hydrogen permeance for Pd/Al_2O_3 hollow fiber composite membrane.

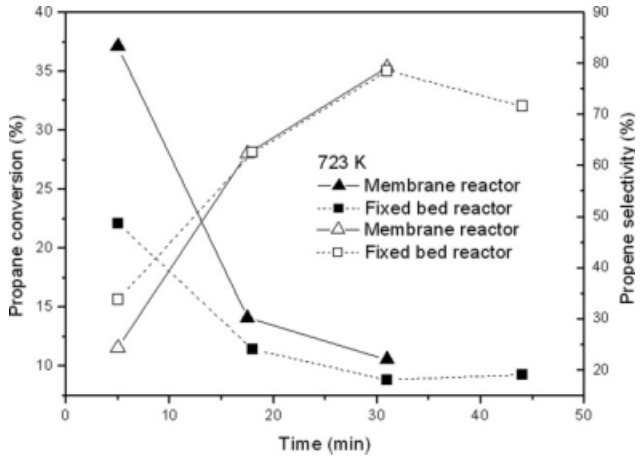

Figure 10. Propane conversion (solid symbols) and propene selectivity (open symbols) of the inorganic hollow fiber membrane reactor (iHFMR) and fixed bed reactor (FBR).

testing the fiber gas tightness developed by Tan et al.[23] was also used, further confirming that the membrane used is gastight.

As can be seen in Figure 8, the hydrogen permeation flux increased with increasing temperature. The linear relationship between the hydrogen flux and the square root of the pressure difference indicated that the pressure exponent (n) is equal to 0.5 in the temperature range of 723–873 K. Therefore, bulk diffusion is the controlling step in hydrogen permeation.[3] The apparent activation energy (E_a) of hydrogen permeation, which was calculated according to the Arrhenius plot shown in Figure 9, was ~5.4 kJ/mol, agreeing well with the reported values of 6.38,[7] 5.73,[24] and 5.7 kJ/mol.[25] However, higher E_a values of 9.8,[21] 11.36,[26] and 15.5 kJ/mol[27] have also been reported, indicating that the E_a value of Pd/Ag membranes is an indication of the net effects of a number of factors. Irrespective to the uniformity of the membrane, the E_a of the Pd/Ag membranes is closely related to the weight ratio between Pd and Ag. For example, Pd/Ag membranes with 20–23 wt % of Ag possess a relatively low E_a. Also, E_a is dependent on the controlling step of the hydrogen permeation. For instance, the E_a value for the hydrogen permeation process controlled by bulk diffusion is lower than that controlled by surface exchange.

Dehydrogenation of propane to propene

The performance of the iHFMR was compared with a FBR, in which 0.1 g of Pt (0.5 wt %)/γ-alumina catalyst was packed into the center of a dense ceramic tube of 9 mm in diameter. As can be seen in Figure 10, the propane conversion in the FBR started at about 22% and then reduced to about 8% after 40 min, which is close to the equilibrium conversion of propane at 723 K. In the mean time, the propene selectivity increased from about 34 to 80%. This trend agrees well with the work of Lobera et al.,[28] in which the coke content increased abruptly in the first ~10 min, causing quick catalyst deactivation at the initial stage of the reaction. In the case of the iHFMRs, the initial propane conversion of the 1st iHFMR was measured to be about 37%, which is ~68% higher than that of the FBR. Similar results listed in Table 3 are also obtained for a 2nd iHFMR, which proves that the use of the iHFMRs substantially shift the reaction to the product side and increase propane conversion. However, as the reaction proceeds, a faster decrease in propane conversion was observed in the iHFMRs, which may be due to the more serious carbon deposition in membrane reactors.[4] This problem may be able to overcome by using coking-resistant catalysts such as Pt-Sn supported catalyst.[29] In commercial dehydrogenation operations, the generation of hydrogen from the reaction serves to reduce carbon formation tendency. Although the removal of generated hydrogen in a membrane reactor contributes to an increase in conversion and yield of the reaction, it aggravates the formation of carbon, which may block the surface of the catalyst, foul the reactor, or even accumulate on the membrane surface, blocking further hydrogen permeation.[4] Instead of removing hydrogen as soon as it forms, a certain amount of hydrogen should be deliberately kept in the reaction zone to mitigate catalyst deactivation, although the conversion of the reaction is reduced at the same time.

Figure 10 further illustrates that the difference in performance between the two reactor designs is diminished as a function of time. One of the possible reasons for this result is that due to the relatively low propane conversion at 723 K, the amount of hydrogen produced in the iHFMRs was small. Hence, limited driving force of the hydrogen can be built up for the hydrogen permeation, leading to the similar performances between iHFMR and FBR. For endothermic

Table 3. Propane Conversion and Propene Selectivity of iHFMRs

	Time (min)	Propane Conversion (%)	Propene Selectivity (%)
1st iHFMR	5	37.16	24.27
	17.5	14.12	62.39
2nd iHFMR	5	35.65	27.92
	16	12.26	75.48
3rd iHFMR	5	42.07	–
	45	6.29	–

Table 4. Space-Time Yields (STY) of the 1st iHFMR and FBR

	STY of iHFMR			STY of FBR	
Time (min)	(mol propene/m^3 h)	(g propene/g catalyst h)	Time (min)	(mol propene/m^3 h)	(g propene/g catalyst h)
5	2488.60	12.82	5	398.62	0.21
17.5	2431.61	12.52	18	379.64	0.20
31	2298.63	11.84	31	366.99	0.19
			44	352.22	0.18

dehydrogenation reactions, the high demand for heat means that the products of reaction can be trapped within the pores of catalyst, resulting in a fast catalyst deactivation as a consequence of carbon deposition.[4] So, it is logical to conclude that hydrogen permeation through the membrane is not the rate limiting process, because the rate of hydrogen production in the catalytic membrane reactor is limited by catalyst productivity.[30] As a result, the use of coking-resistant catalyst with great catalytic activity is critically important to further improve the performance of the membrane reactor. However, because of the high surface area of the asymmetric substrates, comparable propane conversion and propene selectivity were obtained with much less catalyst (around 1.15 mg in the reaction zone) used in the iHFMR compared to that of FBR. Table 4 shows the space-time yields (STY) of the 1st iHFMR and FBR. As can be seen, the STY of the iHFMR is more than six times that of the FBR. It should be noted that this value can be further increased to ~14 when smaller ceramic substrates (OD = 1.3 mm) with similar asymmetric structures are used.[31] Moreover, the STY of the iHFMR, in view of the amount of catalyst used, is more than 60 times that of the FBR, indicating that the iHFMR is more efficient in propene production. This demonstrates another advantage of the iHFMR in propane dehydrogenation.

To further assess the performance of the iHFMR, a 3rd iHFMR was used in propane dehydrogenation using same operating conditions described previously. As shown in Table 3, similar to the other two iHFMRs, the propane conversion of the 3rd iHFMR decreased from 42.07% at 5 min to 6.29% after 45 min as a result of catalyst deactivation. The reactor was then regenerated at 773 K for 2 h, using a stream consisting of 40% of O_2 and 60% of Ar. As shown in Figure 11, after the regeneration, the initial propane conversion was recovered to 38.89%, which is ~8% lower than that of the fresh iHFMR. In addition, the final propane conversion was about 5.54%.

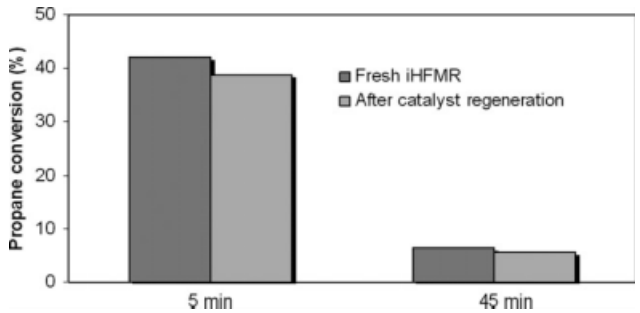

Figure 11. The performance comparison of a third iHFMR in dehydrogenation of propane.

Although high initial propane conversions have been achieved in the iHFMRs, quick catalyst deactivation is still a challenge. To improve the performance of the iHFMR in dehydrogenation reactions, coking-resistant catalysts such as Pt-Sn catalysts with sufficiently great activity at high operating temperatures should be used. Furthermore, the beneficial effect of the highly compact multifunctional iHFMR developed in this study can be used in other catalytic reactions with less coking problems such as steam reforming or water-gas shift (WGS) reactions.

Conclusions

Al_2O_3 hollow fiber substrates with a unique asymmetric structure were prepared by a combined phase inversion/sintering technique. The asymmetric structure consists of long finger-like voids and a uniform outer sponge-like layer of about 60–70 μm in thickness. Based on the analysis, the outer sponge-like layer of the substrate provides a sufficiently smooth surface for direct coating of thin and dense Pd/Ag membranes for hydrogen separation. After depositing submicron-sized Pt (0.5 wt %)/γ-alumina catalyst particles in the finger-like voids, a highly compact multifunctional membrane reactor was developed and applied in dehydrogenation of propane to propene. At the operating temperature of 723 K, the propane conversion as high as 42% was achieved in the iHFMR at the initial stage of the reaction. The advantage of using iHFMR compared to FBR is diminished after 40 min of operation due to the deactivation of the catalyst and the low equilibrium conversion of propane. However, due to the high surface area of the asymmetric substrates, comparable propane conversion and propene selectivity were obtained with much less catalyst used in the case of iHFMR, which clearly demonstrated the advantages of the iHFMR developed.

Acknowledgments

The authors gratefully acknowledge the research funding provided by EPSRC in the United Kingdom (grant No. EP/F027427/1).

Literature Cited

1. Bhasin MM, McCain JH, Vora BV, Imai T, Pujado PR. Dehydrogenation and oxydehydrogenation of paraffins to olefins. *Appl Catal A Gen*. 2001;221:397–419.
2. Ertl G, Knözinger H, Weitkamp J. *Handbook of Heterogeneous Catalysis*. Weinheim: VCH, 1997.
3. Paglieri SN, Way JD. Innovations in palladium membrane research. *Sep Purif Methods*. 2002;31:1–169.
4. Armor JN. Applications of catalytic inorganic membrane reactors to refinery products. *J Membr Sci*. 1998;147:217–233.
5. Weyten H, Luyten J, Keizer K, Willems L, Leysen R. Membrane performance: the key issues for dehydrogenation reactions in a catalytic membrane reactor. *Catal Today*. 2000;56:3–11.

6. Collins JP, Schwartz RW, Sehgal R, Ward TL, Brinker CJ, Hagen GP, Udovich CA. Catalytic dehydrogenation of propane in hydrogen permselective membrane reactors. *Ind Eng Chem Res*. 1996;35: 4398–4405.
7. Yildirim Y, Gobina E, Hughes R. An experimental evaluation of high-temperature composite membrane systems for propane dehydrogenation. *J Membr Sci*. 1997;135:107–115.
8. Uemiya S. State-of-the-art of supported metal membranes for gas separation. *Sep Purif Methods*. 1999;28:51–85.
9. Tan XY, Liu SM, Li K. Preparation and characterization of inorganic hollow fiber membranes. *J Membr Sci*. 2001;188:87–95.
10. Pan XL, Xiong GX, Sheng SS, Stroh N, Brunner H. Thin dense Pd membranes supported on alpha-Al2O3 hollow fibers. *Chem Commun*. 2001;2536–2537.
11. Nair BKR, Harold MP. Pd encapsulated and nanopore hollow fiber membranes: synthesis and permeation studies. *J Membr Sci*. 2007;290:182–195.
12. Nair BKR, Choi J, Harold MP. Electroless plating and permeation features of Pd and Pd/Ag hollow fiber composite membranes. *J Membr Sci*. 2007;288:67–84.
13. Pan XL, Stroh N, Brunner H, Xiong GX, Sheng SS. Pd/ceramic hollow fibers for H-2 separation. *Sep Purif Technol*. 2003;32:265–270.
14. Wang WP, Thomas S, Zhang XL, Pan XL, Yang WS, Xiong GX. H-2/N-2 gaseous mixture separation in dense Pd/alpha-Al2O3 hollow fiber membranes: experimental and simulation studies. *Sep Purif Technol*. 2006;52:177–185.
15. Tong JH, Su LL, Haraya K, Suda H. Thin and defect-free Pd-based composite membrane without any interlayer and substrate penetration by a combined organic and inorganic process. *Chem Commun*. 2006;1142–1144.
16. Tong JH, Su LL, Haraya K, Suda H. Thin Pd membrane on alpha-Al2O3 hollow fiber substrate without any interlayer by electroless plating combined with embedding Pd catalyst in polymer template. *J Membr Sci*. 2008;310:93–101.
17. Sun GB, Hidajat K, Kawi S. Ultra thin Pd membrane on alpha-Al2O3 hollow fiber by electroless plating: high permeance and selectivity. *J Membr Sci*. 2006;284:110–119.
18. Li JS, Wang LJ, Hao YX, Liu XD, Sun XY. Preparation and characterization of Al2O3 hollow fiber membranes. *J Membr Sci*. 2005;256:1–6.
19. Wu L-Q, Xu N, Shi J. Preparation of a palladium composite membrane by an improved electroless plating technique. *Ind Eng Chem Res*. 2000;39:342–348.
20. Shu J, Adnot A, Grandjean BPA, Kaliaguine S. Structurally stable composite Pd-Ag alloy membranes: introduction of a diffusion barrier. *Thin Solid Films*. 1996;286:72–79.
21. Hou K, Hughes R. Preparation of thin and highly stable Pd/Ag composite membranes and simulative analysis of transfer resistance for hydrogen separation. *J Membr Sci*. 2003;214:43–55.
22. Uemiya S, Matsuda T, Kikuchi E. Hydrogen permeable palladium-silver alloy membrane supported on porous ceramics. *J Membr Sci*. 1991;56:315–325.
23. Tan X, Liu Y, Li K. Mixed conducting ceramic hollow-fiber membranes for air separation. *AIChE J*. 2005;51:1991–2000.
24. Yoshida H, Konishi S, Naruse Y. Effects of impurities on hydrogen permeability through palladium alloy membranes at comparatively high-pressures and temperatures. *J Less Common Met*. 1983;89:429–436.
25. Kikuchi E, Jemiya S. Preparation of supported thin palladium-silver alloy membranes and their characteristics for hydrogen separation. *Gas Sep Purif*. 1991;5:261–266.
26. Cheng YS, Peña MA, Fierro JL, Hui DCW, Yeung KL. Performance of alumina, zeolite, palladium, Pd-Ag alloy membranes for hydrogen separation from Towngas mixture. *J Membr Sci*. 2002;204:329–340.
27. Uemiya S, Sato N, Ando H, Kude Y, Matsuda T, Kikuchi E. Separation of hydrogen through palladium thin film supported on a porous glass tube. *J Membr Sci*. 1991;56:303–313.
28. Lobera MP, Téllez C, Herguido J, Menéndez M. Transient kinetic modelling of propane dehydrogenation over a Pt-Sn-K/Al2O3 catalyst. *Appl Catal A Gen*. 2008;349:156–164.
29. de Miguel SR, Jablonski EL, Castro AA, Scelza OA. Highly selective and stable multimetallic catalysts for propane dehydrogenation. *J Chem Technol Biotechnol*. 2000;75:596–600.
30. Matsuda T, Koike I, Kubo N, Kikuchi E. Dehydrogenation of isobutane to isobutene in a palladium membrane reactor. *Appl Catal A Gen*. 1993;96:3–13.
31. Wei CC, Chen OY, Liu Y, Li K. Ceramic asymmetric hollow fibre membranes—one step fabrication process. *J Membr Sci*. 2008;320: 191–197.

Manuscript received Sept. 15, 2008, and revision received Jan. 23, 2009.